A product branching ratio controlled by vibrational adiabaticity and variational effects: Kinetics of the H + *trans*-N$_2$H$_2$ reactions

Jingjing Zheng,[1] Roberta J. Rocha,[2] Marina Pelegrini,[3] Luiz F. A. Ferrão,[2] Edson F. V. Carvalho,[2] Orlando Roberto-Neto,[4] Francisco B. C. Machado,[2] and Donald G. Truhlar[1,a]

[1]*Department of Chemistry and Supercomputing Institute, University of Minnesota, Minneapolis, Minnesota 55455-0431, USA*
[2]*Departamento de Química, Instituto Tecnológico de Aeronáutica, São José dos Campos, 12228-900 São Paulo, Brazil*
[3]*Divisão de Ensino, Academia da Força Aérea, Pirassununga,13643-000 São Paulo, Brazil*
[4]*Divisão de Aerotermodinâmica e Hipersônica, Instituto de Estudos Avançados, São José dos Campos, 12228-001 São Paulo, Brazil*

The abstraction and addition reactions of H with *trans*-N$_2$H$_2$ are studied by high-level *ab initio* methods and density functional theory. Rate constants were calculated for these two reactions by multistructural variational transition state theory with multidimensional tunneling and including torsional anharmonicity by the multistructural torsion method. Rate constants of the abstraction reaction show large variational effects, that is, the variational transition state yields a smaller rate constant than the conventional transition state; this results from the fact that the variational transition state has a higher zero-point vibrational energy than the conventional transition state. The addition reaction has a classical barrier height that is about 1 kcal/mol lower than that of the abstraction reaction, but the addition rates are lower than the abstraction rates due to vibrational adiabaticity. The calculated branching ratio of abstraction to addition is 3.5 at 200 K and decreases to 1.2 at 1000 K and 1.06 at 1500 K. © *2012 American Institute of Physics*. [http://dx.doi.org/10.1063/1.4707734]
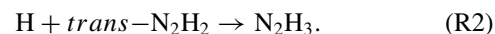
I. INTRODUCTION

The classical barrier height (zero-point-exclusive barrier height) is defined as the potential energy difference between the saddle point (SP) and the reactants. The classical barrier height on a potential energy surface is generally the main factor that controls the rate of a chemical reaction, and therefore it is given much attention when studying reaction mechanisms. However, it has been already shown that the application of variational transition state theory[1-4] (VTST) is also important for the calculation of accurate rate constants. In this theory, a free energy bottleneck is located along the reaction path for each temperature, instead of assuming the transition state is the saddle point, as in conventional transition state theory[5,6] (which will be abbreviated simply as TST). We define the "variational effect" as the difference between the rate calculated by VTST and that calculated by TST. It is important to understand how large the variational effect can be.

Recently, Schreiner *et al.*[7] showed that the isomerization of methylhydroxycarbene does not mainly proceed through the lowest-energy reaction path, but through a higher-energy path due to tunneling contributions at low temperature (11 K). Is it possible that a chemical reaction proceeds mainly through a higher-energy path for other reasons at room temperature or higher temperature? It is well known by now that variational effects can be very large in some cases.[1,8-13] Often such effects are dominated by different vibrational energy requirements at the variational and conventional transition states.

High-frequency vibrational modes are particularly important, since they tend to be vibrationally adiabatic.[14-16]

In this article, results for two reactions will be studied that show the importance of considering the variational effect for the calculation of rate constants and also show that the branching ratios depend not only on the classical barrier heights but also on the full vibrationally adiabatic potential energy curve. The two reactions investigated in this work are

$$\text{H} + trans-\text{N}_2\text{H}_2 \rightarrow \text{N}_2\text{H} + \text{H}_2, \qquad (\text{R1})$$

$$\text{H} + trans-\text{N}_2\text{H}_2 \rightarrow \text{N}_2\text{H}_3. \qquad (\text{R2})$$

In reaction (R1), the reaction H with *trans*-N$_2$H$_2$ proceeds by H abstraction, and in reaction (R2) it proceeds by addition. Both the abstraction and the addition have a barrier.

Chuang *et al.*[17] studied reaction (R1) by using several electronic structure methods based on single-configuration reference states in order to examine the effects of spin contamination on the calculated geometries and energies. They estimated that the classical barrier height ($V^{\ddagger}$) is in the range from 3 to 5 kcal/mol, and the reaction energy (ΔE) is in the range from -37 to -38 kcal/mol. At the MP2 level, they found large differences (5–7 kcal/mol) between the results calculated with unrestricted and restricted reference states, but when using coupled cluster theory with single and double excitations and quasiperturbative inclusion of connected triples[18] (CCSD(T)) these differences were only tenths of a kcal/mol.

In a more recent study, Lynch and Truhlar[19] built an energetic database for some benchmark hydrogen abstraction

a)Authors to whom correspondence should be addressed. Electronic addresses: orlando@ieav.cta.br and truhlar@umn.edu.

reactions. For the reaction under consideration, the values of $V^{\ddagger}$ and ΔE were estimated to be 5.9 and -35.1 kcal/mol, respectively, differing significantly from the previous estimates. Because of the uncertainty, this reaction was later dropped from the database.[20]

There are no experimental rate constants available for H + *trans*-N_2H_2. Previous theoretical works focused only on the abstraction reaction (R1). Theoretical rate constants include VTST calculations performed with MRCI//CASSCF/cc-pVDZ data,[21] VTST calculations with MRCI/CASSCF/cc-pVDZ///NDDO-SRP data and rectilinear[22] or curvilinear[23] internal coordinates, and TST calculations with G2M(MP2)//MP2/6-31G(*d*,*p*) data.[24] The values employed for the classical barrier height and reaction energy are 5.9 and -33.6 kcal/mol (Refs. 20–23) and 4.1 and -37.5 kcal/mol.[24] The potential energy surfaces used in these rate calculations are not reliably accurate, and dual-level direct dynamics[22,25] was employed[22] to try to improve the accuracy. We will show that the description of these reactions will be qualitatively different when we use a higher-quality potential energy surface.

In the present study we performed high-level *ab initio* calculations to obtain best estimate barrier heights (benchmarks) of both the abstraction and addition reactions. Single-level direct dynamics (eliminating approximations in dual-level dynamics) calculations including multistructural variational effects[26] were performed using potential energy surfaces calculated by density functional theory with functionals that are validated against the benchmark calculations. In the dynamics calculations, we also include the torsional anharmonicity using our recent developed multistructural method.[26,27]

It is well known that there are three isomers of diazene (N_2H_2), but the *trans*-N_2H_2 species is, respectively, 5.1 and 24.0 kcal/mol more stable than the *cis*- and *iso*-N_2H_2 isomers.[28] The present article is concerned only with the *trans*-isomer.

II. METHODS

II.A. Electronic structure

Both reactions are known to be very exothermic from previous studies.[20–24] Here, reactants and transition states are optimized by CCSD(T) using the cc-pVTZ (Ref. 29) basis set and by the M08-SO (Ref. 30) density functional with two triple ζ basis sets, ma-TZVP (Ref. 31) and 6-311++G(2*df*,2*p*). Single-point energies are calculated by CCSD(T) with explicit correlation, in particular, CCSD(T)-F12a and CCSD(T)-F12b,[32,33] and by various multireference methods (multireference configuration interaction with single and double excitations (MRCI),[34,35] MRCI with the Davidson correction (MRCI+Q),[36,37] multireference averaged coupled pair functional (MR-ACPF),[38,39] and multireference averaged quadratic coupled cluster (MR-AQCC) (Refs. 39 and 40)) using CCSD(T)/cc-pVTZ geometries. In the multireference calculations, the active space includes 13 electrons in 12 orbitals.

As usual, the Born-Oppenheimer (BO) energy E is defined as electronic energy plus nuclear repulsion. The BO energy as a function of nuclear coordinates is the potential energy surface used for dynamics. The calculated energetic properties are the BO energy of reaction (ΔE), the enthalpy of the reaction at 0 K (ΔH_0°), the classical barrier height ($V^{\ddagger}$) (defined as the BO energy difference between the SP and the reactants), and the ground-state vibrationally adiabatic barrier height evaluated at the conventional transition state, $\Delta V_a^{\mathrm{G}\ddagger}$, for the forward reaction ($\Delta V_a^{\mathrm{G}\ddagger}$ is defined as $V^{\ddagger}$ plus the change in zero-point energy in proceeding from reactant to the SP).

Because of the multireference character, we tested the sensitivity of the coupled cluster results to variations in the choice of orbitals and spin adaptation; in particular, we tested five possibilities: (1) UU type (also called spin-unrestricted or U type): the orbitals are obtained by unrestricted Hartree–Fock (HF), and the resulting CCSD and CCSD(T) calculations are also unrestricted. (2,3) RU type: the orbitals are obtained by spin-restricted HF (2) or spin-restricted Kohn-Sham (KS) (3) calculations (for open-shells these are sometimes labeled ROHF and ROKS, respectively), but the CCSD and CCSD(T) results are spin unrestricted. (4,5) RR type: the orbitals are obtained by spin-restricted HF (4) or restricted Kohn-Sham (5) calculations, and the CCSD and CCSD(T) calculations are partially spin-adapted.

In some cases, energies were extrapolated to the complete basis set (CBS) limit by using the extrapolation procedure of Halkier *et al.*,[41]

$$E_{\mathrm{CBS}} = \frac{n^3 E(n) - (n-1)^3 E(n-1)}{n^3 - (n-1)^3}, \tag{1}$$

where n is the ζ level of the largest cc-pVnZ basis set used ($n = 4$ in the present work). Equation (1) was also used to extrapolate bond distances, bond angles, and vibrational frequencies.

The 1s core orbitals of the N atom were frozen in the above calculations, which are therefore denoted as frozen-core (FC) calculations. In further calculations, core correlation was included by the CCSD(T) method correlating all electrons ("full") with the correlation consistent polarized core and valence triple zeta basis sets (cc-pCVTZ) of Woon and Dunning.[42] The best estimate (BE) values were computed based on a method advocated by Martin and Taylor,[43] in particular, by using

$$\begin{aligned} E_{\mathrm{BE}} = {} & E_{\mathrm{CBS}}(\mathrm{FC}) + E(\mathrm{cc-pCVTZ, full}) \\ & - E(\mathrm{cc-pCVTZ, FC}). \end{aligned} \tag{2}$$

The M08-SO density functional is used with the ma-TZVP and 6-311++G(2*df*,2*p*) basis sets for straight direct dynamics calculations for both reactions. The grid for density functional integration has 96 radial shells around each atom and a spherical product angular grid having 32 θ points and 64 φ points in each shell.

II.B. Dynamics

In straight direct dynamics calculations, minimum energy paths (MEPs) in isoinertial coordinates are calculated using a variational reaction path[44] algorithm from 0.2 to -1.0 Å for reaction (R1) and from 0.3 to -0.6 Å for reaction (R2). The step size was 0.002 Å, and Hessians were calculated each 9 steps. Note that we set the reduced mass μ equal to 1 amu and isoinertial coordinates have the unit of length (we use Å). Vibrational frequencies were computed in curvilinear coordinates and were scaled by a factor[45] 0.984.

The multistructural canonical VTST rate constants (MS-CVT) (Ref. 26) were combined with the zero-curvature tunneling (ZCT) (Refs. 9, 46, and 47) and small-curvature tunneling (SCT) (Refs. 47 and 48) approximations. Torsional anharmonicity was included by using the multistructural torsion (MS-T) method.[26, 27] Note that "multistructural" means that multiple conformational structures are included for a stationary point, and the number of the conformational structures is in general larger than 1 (if it were 1, we would use the original single-structure version of the theory). By default, we include all the structures, and in this article we do include them all. We define the anharmonicity factor as the ratio of the multistructural conformational-rotational-vibrational partition function[27] to the single-structure harmonic-oscillator rotational-vibrational partition function:

$$F = \frac{Q_{\text{con-rovib}}^{\text{MS-T}}}{Q_{\text{rovib}}^{\text{HO}}}, \qquad (3)$$

where $Q_{\text{con-rovib}}^{\text{MS-T}}$ is the conformational-rovibrational partition function calculated by the MS-T method,[27] and $Q_{\text{rovib}}^{\text{HO}}$ is the rovibrational partition function calculated by the single-structure rigid-rotor harmonic oscillator formulas. Further details of the anharmonicity factor calculation can be found in Refs. 27 and 52.

The electronic structure calculations were carried out with the GAUSSIAN 09 (Ref. 49) and MOLPRO (Ref. 50) quantum chemistry codes. Thermal rate constants were calculated by employing the POLYRATE code, version 2010-A,[51] and multistructural anharmonicity was calculated with the MSTOR (Ref. 52) code.

For the association reaction (R2), we assume that the pressure is sufficiently high to stabilize the initially formed internally energetic N_2H_3 so that it will not redissociate to H and N_2H_2.

III. RESULTS AND DISCUSSION

III.A. Multireference character

An important issue in our recent work[53–56] has been to study the applicability of various electronic structure methods to reactions that have large multireference character. The present reaction provides another problem where this is important. We therefore begin by attempting to quantify the multireference character.

We estimated the importance of non-dynamical correlation effects in the electronic wave function by using the T_1 diagnostic[57] and employing the GAUSSIAN and MOLPRO

codes in unrestricted reference and restricted open-shell reference calculations, respectively. It has been argued that the multireference wave function character is significant only if the T_1 diagnostic value is greater than 0.044.[58] Using the UU-CCSD(FC) method with the cc-pVQZ basis set, the computed values of T_1 are 0.012, 0.001, 0.044, and 0.027 for the N_2H_2, H_2, N_2H, and SP of R1 (SP_{R1}) species, respectively. For the open-shell species N_2H and SP_{R1}, the values of T_1 change to 0.026 and 0.029 using the RU-CCSD/cc-pVQZ method. From these values we can infer that the multireference character of N_2H and SP_{R1} is marginal and that of the other species is very small. One can also estimate the multireference character of the electronic wave functions using the CASSCF and MRCI methods. The multireference M diagnostic[54] calculated using CASSCF/cc-pVQZ for N_2H_2, H_2, N_2H, and SP_{R1} are equal to 0.086, 0.025, 0.083, and 0.086, respectively. As pointed out previously,[54] values of the M diagnostic smaller than 0.05 and equal to 0.05–0.10 are considered to have, respectively, a small and modest multireference character, so by this criterion the multireference character is modest. Also, the MRCI/cc-pVQZ wave functions of the reactants, products, and transition state are highly but not completely dominated by the HF reference configuration, i.e., the coefficients of the HF are 0.93, 0.99, 0.93, and 0.92 for N_2H_2, H_2, N_2H, and SP_{R1}, respectively. This confirms the non-negligible multireference character in N_2H_2, N_2H, and SP_{R1}.

The value of T_1 for the SP of reaction (R2) as calculated by the RU-CCSD/aug-cc-pVQZ with HF orbitals is 0.022, which is less than that of the SP of R1. This indicates that reaction (R2) has less multireference character.

III.B. Potential energy surface features of R1

Calculated equilibrium geometries and vibrational frequencies of SP_{R1} are given in Tables I and II, respectively, while all the other structures (reactants and products) of R1 are given in the supplementary material. There is only one distinguishable structure for the SP of the reaction (R1) (see Fig. 1). Due to the low barrier height and high exoergicity of this reaction (which will be documented in Tables III and IV) and as expected from Hammond's postulate,[59] the extension of the forming H–H bond is larger than that of the breaking H–N bond, as shown in the first two columns of Table I. The CCSD(T)/CBS geometry obtained by the geometrical analog of Eq. (1) has tighter breaking bonds and looser forming bonds than does the CASSCF/CBS geometry obtained the same kind of basis-set extrapolation. The CCSD(T) geometries are more reliable than those obtained by CASSCF.

The best-estimated equilibrium geometries of N_2H_2, N–H (1.243 Å), N–N (1.028 Å), and ∠HNN (106.4°), are in excellent agreement with experimental values, i.e., 1.247 Å, 1.030 Å, and 106.3°, respectively.

The scaled M08-SO/ma-TZVP frequencies have a good agreement with unscaled frequencies calculated by the CCSD(T)/CBS method plus core-valence correlation (CV). CASSCF overestimates the harmonic frequencies as compared to CCSD(T). For instance, the values of the imaginary

TABLE I. Bond distances (Å) and angles (deg) of the R1 saddle point.[a]

Methods	4H–2N	4H–5H	N–N	3H–1N	3H–N–N	4H–N–N	5H–4H–N
M08-SO/ma-TZVP	1.104	1.270	1.216	1.038	108.3	108.0	170.8
M08-SO/6-311++G(2*df*,2*p*)	1.106	1.259	1.216	1.038	108.4	108.1	170.2
CASSCF/cc-pVTZ	1.163	1.177	1.238	1.047	106.5	106.7	172.8
CASSCF/cc-pVQZ	1.164	1.172	1.236	1.046	106.7	106.9	172.5
CASSCF/CBS	1.165	1.168	1.235	1.045	106.9	106.9	172.3
CCSD(T)(FC)/cc-pVTZ	1.143	1.218	1.233	1.033	106.5	106.5	171.5
CCSD(T)(FC)/cc-pVQZ	1.111	1.205	1.228	1.032	106.9	106.8	171.3
CCSD(T)(AE)/cc-pCVTZ	1.107	1.218	1.229	1.032	106.6	106.7	171.2
CCSD(T)/cc-pCVTZ	1.107	1.219	1.232	1.033	106.5	106.5	171.5
CCSD(T)(FC)/CBS (Eq. (1))	1.114	1.196	1.224	1.032	107.2	106.9	171.2
CCSD(T)/CBS+CV(Eq. (2))	1.114	1.195	1.222	1.030	107.3	107.1	171.0

[a]The atoms are labeled as 5H···4H–2N–1N–3H.

frequencies, which give information about the shape at the top of the reaction barrier, are 2600*i* cm^{-1} and 1503*i* cm^{-1} calculated by the CASSCF/CBS and the CCSD)(T)/CBS+CV methods, respectively.

Table III lists the single-point barrier height and reaction energy (in kcal/mol) calculated with the geometries obtained by the CCSD(T)/CBS+CV method and using various combinations of spin restrictions and various methods to obtain orbitals for CCSD(T) calculations. RU-CCSD(T) results with either a HF reference or a KS reference give forward barriers between 2.9 and 3.0 kcal/mol, but the UU-CCSD(T) calculations with HF orbitals give a higher barrier, 3.3 kcal/mol. The RR-CCSD(T) and RU-CCSD(T) results depend more on the reference orbitals than do the UU-CCSD(T) results. For instance, the RR-CCSD(T)/cc-pVTZ method with HF orbitals gives a 3.5 kcal/mol barrier, while the RR-CCSD(T)/cc-pVTZ method with B3LYP orbitals gives a 3.1 kcal/mol barrier. The predicted barrier heights by CCSD(T) methods using various orbitals fall into the range of 2.9–3.5 kcal/mol.

The forward reaction barrier heights of reaction (R1) calculated by coupled cluster and multireference methods are listed in Table IV. These are single-point calculations using the CCSD(T)/cc-pVTZ geometries. There is a good agreement between the values of the classical barrier height computed by the MRCI+Q and RU-CCSD(T)-F12 methods us-

ing HF orbitals. The MR-ACPF calculations give slightly higher barrier (in the range of 0.1–0.2 kcal/mol) than the RU-CCSD(T)-F12 method.

More information on barrier heights, reaction energies, and geometries are given in supplementary material.[60]

III.C. Potential energy surface features of R2

Table V lists a set of geometry parameters of the reaction (R2) SP. Note that the SP of reaction (R2) has a pair of mirror images that are distinguishable structures (see Fig. 1). Also note that the mirror images of a stationary point are the same in energetics (energies and vibrational frequencies) and therefore Tables IV and VI are valid for the both structures, which are both included in the MS-T treatment. Table VI lists harmonic vibrational frequencies of reaction (R2) SP, which are unscaled frequencies whereas in dynamics calculations scaled frequencies with a scaling factor[45] of 0.984 are used for M08–SO/ma-TZVP and M08–SO/6-311++G(2*df*,2*p*) methods, respectively. The scaling factor 0.984 for M08–SO/6-311++G(2*df*,2*p*) method is parameterized against the ZPE15/10 database[45] in this work.

The N_2H_2 geometry does not have significant changes at the R2 SP, which indicate an early transition state for this

TABLE II. Harmonic vibrational frequencies (cm^{-1}) of the R1 saddle point.[a]

Methods	Vibrational frequencies								
M08-SO/ma-TZVP	3228	1821	1628	1479	1291	1276	459	307	1465*i*
M08-SO/6-311++G(2*df*,2*p*)	3256	1801	1608	1475	1283	1266	460	310	1603*i*
CASSCF/cc-pVTZ	3553	1617	1519	1348	1284	1227	581	394	2559*i*
CASSCF/cc-pVQZ	3553	1619	1515	1349	1282	1227	579	392	2583*i*
CASSCF/CBS	3553	1620	1512	1350	1281	1227	578	391	2601*i*
CCSD(T)(FC)/cc-pVTZ	3264	1723	1587	1500	1315	1298	515	356	1345*i*
CCSD(T)(AE)/cc-pCVTZ	3257	1723	1580	1490	1308	1298	468	329	1370*i*
CCSD(T)/cc-pCVTZ	3251	1718	1578	1488	1305	1298	465	328	1365*i*
CCSD(T)(FC)/cc-pVQZ	3268	1713	1573	1490	1310	1287	513	367	1433*i*
CCSD(T)(FC)/CBS[b]	3270	1706	1562	1483	1306	1280	512	376	1498*i*
CCSD(T)/CBS+CV[c]	3275	1711	1563	1485	1308	1280	514	376	1503*i*

[a]All the frequencies in this table are not scaled. But the M08-SO/ma-TZVP frequencies are scaled by a factor of 0.984 in the rate calculations.
[b]Equation (1).
[c]Equation (2).

TABLE III. Single-point barrier height and reaction energy (in kcal/mol) for R1 calculated with the (BE) (Eq. (2)) geometries and using various wave functions as reference for CCSD(T) calculations.

Method	Type[a]	Orbitals	ΔE	$V^{\ddagger}$
CCSD(T)/cc-pVTZ	RR	B3LYP	−37.8	3.1
CCSD(T)/cc-pVQZ	RR	B3LYP	−37.6	3.1
CCSD(T)/cc-pVQZ	RR	B3LYP	−37.4	3.1
CCSD(T)/cc-pVTZ	RU	B3LYP	−38.1	2.9
CCSD(T)/cc-pVQZ	RU	B3LYP	−37.8	2.9
CCSD(T)/cc-pVQZ	RU	B3LYP	−37.6	2.9
CCSD(T)/cc-pVTZ	RR	VSXC	−37.8	3.2
CCSD(T)/cc-PVQZ	RR	VSXC	−37.5	3.2
CCSD(T)/CBS	RR	VSXC	−37.3	3.1
CCSD(T)/cc-pVTZ	RU	VSXC	−38.1	2.9
CCSD(T)/cc-pVQZ	RU	VSXC	−37.8	2.9
CCSD(T)/CBS	RU	VSXC	−37.6	2.9
CCSD(T)/cc-pVTZ	RR	HF	−37.7	3.5
CCSD(T)/cc-pVQZ	RR	HF	−37.4	3.5
CCSD(T)/CBS	RR	HF	−37.2	3.5
CCSD(T)/cc-pVTZ	RU	HF	−38.0	3.0
CCSD(T)/cc-pVQZ	RU	HF	−37.5	3.0
CCSD(T)/CBS	RU	HF	−37.1	2.9
CCSD(T)/cc-pVTZ	UU	HF	−37.8	3.3
CCSD(T)/cc-pVQZ	UU	HF	−37.5	3.3
CCSD(T)/CBS	UU	HF	−37.3	3.3

[a]RR denotes restricted DFT orbitals or restricted HF orbitals combined with restricted CCSD(T) and calculated with the MOLPRO code. RU denotes restricted DFT orbitals or restricted HF orbitals combined with unrestricted CCSD(T) and calculated with the MOLPRO code. UU denotes unrestricted HF combined with unrestricted CCSD(T) and calculated with the GAUSSIAN 09 code.

TABLE IV. Forward reaction barrier heights (in kcal/mol) calculated by coupled cluster methods and multireference methods.[a]

Method[b]	R1	R2
CCSD(T)/cc-pVTZ	2.95	2.20
CCSD(T)-F12a/aug-cc-pVTZ	2.77	1.83
CCSD(T)-F12b/aug-cc-pVTZ	2.86	1.88
CCSD(T)-F12b/aug-cc-pVQZ	2.94	1.89
MRCI/aug-cc-pVTZ	4.21	3.00
MRCI+Q/aug-cc-pVTZ	2.81	1.90
MR-ACPF/aug-cc-pVTZ	2.91	2.09
MR-AQCC/aug-cc-pVTZ	3.19	2.28
MRCI/aug-cc-pVQZ	4.38	2.99
MRCI+Q/aug-cc-pVQZ	2.96	1.89
MR-ACPF/aug-ccp-pVQZ	3.04	2.06
MR-AQCC/aug-cc-pVQZ	3.33	2.26
M08-SO/ma-TZVP	2.95	2.12
M08-SO/6-311++G(2*df*,2*p*)	3.06	1.92

[a]Except M08-SO/ma-TZVP method, all other calculations use CCSD(T)/cc-pVTZ geometries.
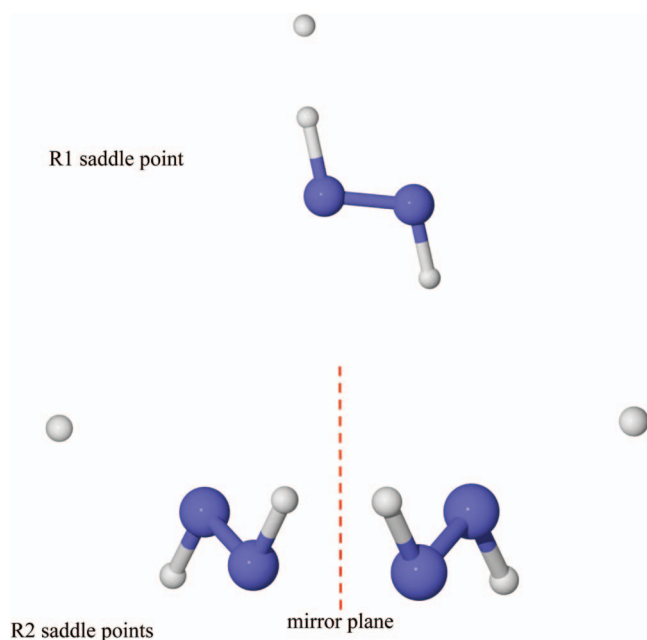[b]All CCSD(T) calculations in this table are of the RU type with HF orbitals.

FIG. 1. Saddle point structures of reactions R1 and R2.

reaction. The DFT geometries agree with CCSD(T)/cc-pVTZ geometries reasonably well.

The forward reaction barrier heights of reaction (R2) calculated by DFT, coupled cluster methods, and multireference methods are listed in Table IV. The barrier heights calculated by coupled cluster methods and multireference methods are between 1.83 and 3.00 kcal/mol. Coupled cluster methods give lower barrier heights than multireference methods. The barrier heights calculated by M08-SO/ma-TZVP and M08–SO/6–311++G(2*df*,2*p*) methods both agree with those calculated by coupled cluster and MRCI+Q methods. Since the T_1 diagnostic of the R2 SP is 0.024, and the barrier heights calculated by coupled cluster and MRCI+Q methods are very close, it seems that these results are the most reliable R2 barrier height.

III.D. Statistical mechanics and chemical kinetics

The barrier heights of R1 and R2 calculated by the density functional M08-SO with either ma-TZVP or 6-311++G(2*df*,2*p*) basis set agree with the benchmark calculations very well. The difference between the barrier heights of R1 and R2 is 0.83 kcal/mol by M08–SO/ma-TZVP method and 1.14 kcal/mol by M08-SO/6-311++G(2*df*,2*p*) method, respectively. Therefore, the difference between two barriers could lead to the branching ratio change, especially at low temperatures. Therefore, both methods (M08–SO/ma-TZVP

TABLE V. Bond distances (Å) and angles (deg) of the R2 saddle point.[a]

Methods	4H–2N	2N–5H	N–N	3H–1N	3H–N–N	4H–N–N	5H–2N–1N
M08-SO/ma-TZVP	1.034	1.873	1.236	1.035	107.7	108.4	120.6
M08-SO/6-311++G(2*df*,2*p*)	1.034	1.875	1.237	1.034	107.7	108.4	120.4
CCSD(T)/cc-pVTZ	1.029	1.897	1.256	1.030	106.0	107.0	121.3

[a]The atoms are labeled as 5H···4H–2N–1N–3H.

TABLE VI. Harmonic vibrational frequencies (cm^{-1}) of the R2 saddle point.[a]

Methods	Vibrational frequencies								
M08-SO/ma-TZVP	3310	3278	1643	1546	1327	1286	425	378	937i
M08-SO/6-311+G(2*df*,2*p*)	3325	3293	1637	1546	1324	1283	409	372	916i
CCSD(T)/cc-pVTZ	3323	3291	1592	1517	1335	1292	377	337	748i

[a]All the frequencies in this table are not scaled. But the M08-SO/ma-TZVP and M08-SO/6-311++G(2df,2p) frequencies are scaled by a factor of 0.984 in the rate calculations.

and M08-SO/6-311++G(2*df*,2*p*)) are used in the dynamics and kinetics calculations for comparison. Since they give similar results, we give the kinetics data by the M08-SO/6-311++G(2*df*,2*p*) method in the article and the data by M08–SO/ma-TZVP method is given in supplementary material.

Table VII lists anharmonicity factors for the two transition states and for the N_2H_2 reactant.

The reactant N_2H_2 has two minima connected by torsion around the N=N bond. As mentioned before, *cis*-N_2H_2 is much higher in energy than *trans*-N_2H_2, (in particular, it is ~5 kcal/mol higher, as compared to, for example, a value of k_BT of ~1 kcal/mol at 500 K), and we only include *trans*-N_2H_2 contribution in the partition function, but we still include a torsional anharmonicity correction for the *trans*-N_2H_2 conformational structure by setting the local periodicity of the N–N torsion equal to 2 in the MS-T calculations. Because the torsional barrier between the two N_2H_2 conformers is quite high (over 50 kcal/mol),[28] the anharmonicity factor FN_2H_2 in Table VII only slightly deviates from 1. The high barrier between two conformers also makes the MS-CVT treatment with only the *trans* conformer valid because the rate of converting two N_2H_2 conformers is much slower than the rate of the reactions studies here.

The abstraction reaction (R1) only has only one SP. Although N_2H_2 has two equivalent hydrogen atoms, and a hydrogen atom can react with either of them, the structures of SP are indistinguishable and they should only be counted once. In the literature, there is a recurrent confusion about this point, and at least one[24] incorrect treatment; therefore, it should be emphasized that we need to count the number of distinguish-

TABLE VII. Anharmonicity factors of Eq. (3) for the two saddle points and N_2H_2.[a]

T (K)	TS1	TS2	N_2H_2
200	1.17	2.01	1.00
250	1.15	2.01	1.00
298	1.12	2.01	1.00
350	1.09	2.01	1.01
400	1.06	2.01	1.01
500	1.00	2.02	1.01
600	0.95	2.02	1.01
700	0.91	2.02	1.01
800	0.87	2.03	1.01
900	0.83	2.03	1.01
1000	0.80	2.03	1.02
1400	0.71	2.05	1.02
1500	0.69	2.06	1.03

[a]The calculations in this table were carried out by M08-SO/6-311++G(2*df*,2*p*) method.

able structures of reactants and SPs instead of counting number of equivalent reactive atoms. Let us consider two reactions as examples for further illustration; one is a H atom abstracting a methyl H in methanol, and the other one is a H atom abstracting a hydrogen atom from ethane. There are three equivalent methyl H atoms in the methanol molecule, and H + methanol can form three distinguishable SPs. However, H + ethane only has one distinguishable SP although there are six equivalent H atoms in ethane.

We considered torsional corrections for the two torsions of the abstraction SP, namely, the H–H–N–N torsion and the H–N–N–H torsion. The former torsion has a very small torsional barrier (estimated as 0.2 kcal/mol by Eq. (13) in Ref. 27) that is larger than k_BT when T < 100 K; therefore, the anharmonicity factor F^{TS1} is slightly larger than 1 at low temperature and it decreases rapidly when the temperature is increased; for example, at 400 K and 500 K it has values of 1.06 and 1.00, respectively.

The addition reaction (R2) has two distinguishable SPs and they are mirror images of each other. Note that these two distinguishable structures exist because of the internal rotation of N–N bond rather than because there are two equivalent N atoms. The two structures are separated by a high barrier (effective barrier 31 kcal/mol given by Eq. (13) in Ref. 27) in the H–N–N–H torsion. Therefore, the anharmonicity factor FTS2 is mainly from the conformational contribution and is very close to 2.

Table VIII lists the reaction rate constants of R1 and R2. All the rate constants include torsional anharmonicity using the multistructural method.[27] The abstraction reaction shows a very large variational effect, especially at low temperatures; the ratio of the TST rate to the CVT rate is 5 at $T = 200$ K, and this ratio approaches to 1 when temperature is increased. What causes this large variational effect? Figure 2 shows the eight vibrational frequencies (the reaction coordinate component is projected out) of the generalized transition state along reaction path. For R1, two modes (red dashed line and green solid line) have a clear crossing around SP. One mode (red dashed line) significantly increases by more than 1000 cm^{-1} over 9 steps (0.018 Å) from the SP toward reactant. This largely increasing vibrational frequency causes a significantly decreasing vibrational partition function of the generalized transition state. Meanwhile, the changes of potential energy from $s = 0.0$ Å to $s = -0.10$ Å are less than 0.15 kcal/mol. Therefore, two factors cause the large variational effect for the abstraction reaction: (i) significantly decreasing vibrational partition functions near the SP and (ii) a very flat potential energy surface around SP. These two changes are reflected on the vibrationally adiabatic ground

TABLE VIII. Calculated reaction rate constants (in cm^3 molecule^{-1} s^{-1}) using M08–SO/6–311++G($2df$,$2p$) potential energy surface.

T (K)	TST	CVT	CVT/ZCT	CVT/SCT
	R1: H + *trans*-N$_2$H$_2$ → N$_2$H + H$_2$			
200	1.02×10^{-12}	1.81×10^{-13}	7.08×10^{-13}	1.13×10^{-12}
250	2.18×10^{-12}	5.83×10^{-13}	1.41×10^{-12}	1.98×10^{-12}
298	3.62×10^{-12}	1.26×10^{-12}	2.36×10^{-12}	3.04×10^{-12}
350	5.45×10^{-12}	2.34×10^{-12}	3.68×10^{-12}	4.46×10^{-12}
400	7.41×10^{-12}	3.70×10^{-12}	5.21×10^{-12}	6.06×10^{-12}
500	1.18×10^{-11}	7.23×10^{-12}	8.94×10^{-12}	9.89×10^{-12}
600	1.67×10^{-11}	1.16×10^{-11}	1.34×10^{-11}	1.44×10^{-11}
700	2.21×10^{-11}	1.70×10^{-11}	1.88×10^{-11}	1.98×10^{-11}
800	2.80×10^{-11}	2.26×10^{-11}	2.30×10^{-11}	2.39×10^{-11}
900	3.42×10^{-11}	2.88×10^{-11}	2.85×10^{-11}	2.94×10^{-11}
1000	4.09×10^{-11}	3.52×10^{-11}	3.43×10^{-11}	3.53×10^{-11}
1400	7.06×10^{-11}	6.43×10^{-11}	6.11×10^{-11}	6.20×10^{-11}
1500	7.94×10^{-11}	7.20×10^{-11}	6.87×10^{-11}	6.93×10^{-11}
	R2: H + *trans*-N$_2$H$_2$ → N$_2$H$_3$			
200	5.78×10^{-14}	5.16×10^{-14}	2.72×10^{-13}	3.22×10^{-13}
250	2.40×10^{-13}	2.14×10^{-13}	6.14×10^{-13}	6.90×10^{-13}
298	6.18×10^{-13}	5.48×10^{-13}	1.14×10^{-12}	1.24×10^{-12}
350	1.32×10^{-12}	1.16×10^{-12}	1.94×10^{-12}	2.08×10^{-12}
400	2.32×10^{-12}	2.02×10^{-12}	2.96×10^{-12}	3.12×10^{-12}
500	5.34×10^{-12}	4.54×10^{-12}	5.68×10^{-12}	5.86×10^{-12}
600	9.75×10^{-12}	8.13×10^{-12}	9.23×10^{-12}	9.47×10^{-12}
700	1.55×10^{-11}	1.27×10^{-11}	1.35×10^{-11}	1.38×10^{-11}
800	2.26×10^{-11}	1.81×10^{-11}	1.85×10^{-11}	1.87×10^{-11}
900	3.08×10^{-11}	2.42×10^{-11}	2.40×10^{-11}	2.42×10^{-11}
1000	4.03×10^{-11}	3.10×10^{-11}	3.00×10^{-11}	3.02×10^{-11}
1400	8.80×10^{-11}	6.37×10^{-11}	5.75×10^{-11}	5.77×10^{-11}
1500	1.02×10^{-10}	7.30×10^{-11}	6.50×10^{-11}	6.54×10^{-11}

FIG. 3. Minimum energy curve (V_{MEP}) and vibrationally adiabatic potential curve (V_a^G) of R1 and R2 calculated by the M08-SO/6-311+G($2df$,$2p$) method.

state energy curves as shown in Fig. 3. Note that the vibrationally adiabatic ground state energy curve is the same as the free energy curve at $T = 0$ K. At finite temperature, the free energy curve differs from V_a^G curve and the location of variational tra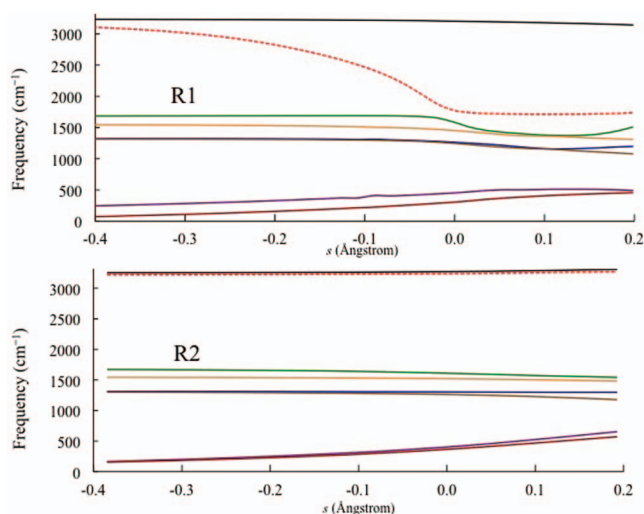nsition state is determined by the maximum of free energy curve. However, it is convenient to explain the variational effect based on V_a^G curve as vibrationally adiabatic ground state energy is a major effect.

The addition reaction (R2) has a small variational effect at low temperatures, i.e., the CVT rate constants are only slightly lower than the TST rate constants. At very high temperature, e.g., $T = 1500$ K, the variational effect becomes more significant. The CVT rate at 1500 K is lower than the TST one by a factor of 1.4. This variational effect is caused by the increase of the two lowest vibrational modes on the product side (see Fig. 2). But this variational effect is not as large as for the abstraction reaction because the increase of the frequencies of the two lowest modes is not as rapid as that for one mode in the abstraction reaction.

It is interesting to note that R2 has lower classical barrier than R1 by $0.8 - 1.1$ kcal/mol, but the reaction rates of R2 are much smaller than those of R1, especially at low temperatures. For example, the CVT/SCT rate for R2 is smaller than the CVT/SCT rate for R1 by about a factor of 6 at 200 K. Figure 4 shows the branching ratio of R1 and R2 using

FIG. 2. Vibrational frequencies of R1 and R2 as functions of the reaction coordinate s. The frequencies are calculated by M08-SO/6-311++G($2df$,$2p$) method with scaling factor 0.984. The curvilinear coordinates are used along the MEP with the variational reaction path algorithm.
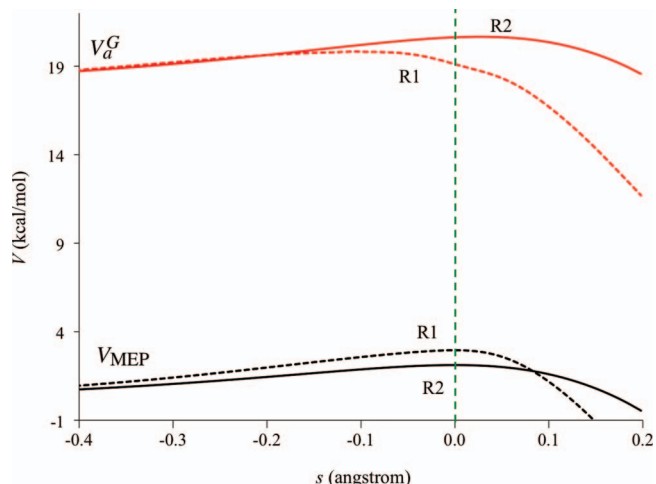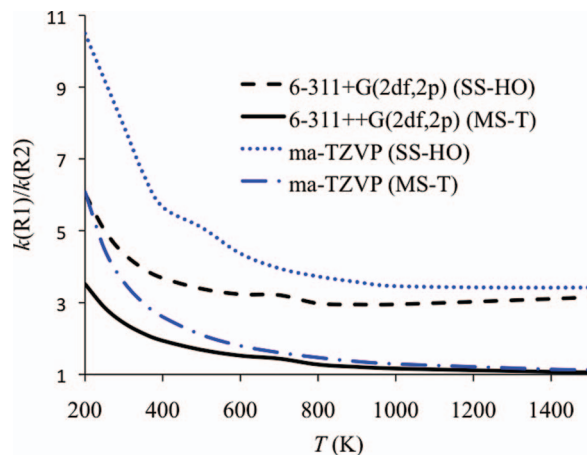

FIG. 4. Branching ratio of the H + *trans*-N$_2$H$_2$ reactions (R1) and (R2) with potential energy surfaces calculated by the M08-SO density functional with two basis sets.

the CVT/SCT method with either single-structure harmonic oscillator approximation or multistructural approximation including torsional anharmonicity (MS-T). Figure 4 also shows the branching ratios calculated by potential energy surfaces calculated by both M08-SO/ma-TZVP and M08-SO/6-311+G(2*df*,2*p*) methods.

Why does the H + *trans*-N$_2$H$_2$ reaction proceed predominantly to produce the product that requires surmounting a higher potential energy barrier? The answer is that the effective barrier has a quantized vibrational energy component as well as a potential energy component. Therefore, Fig. 3 shows that R2 has a higher vibrationally adiabatic ground state energy barrier (the barrier on the V_a^G curve) because R2 has much higher zero-point energy than R1 around the SP. The harmonic vibrational frequencies of R1 and R2 are very similar around the SP except for one mode (red dashed line in Fig. 2). This mode starts as the symmetrical N–H stretching vibration of N$_2$H$_2$ molecule. In R2, this mode does not change much at the transition state. However, this symmetrical N–H stretching vibration becomes a quasisymmetrical N–H and N–N stretching mode at the R1 transition state, and its frequency decreases by about 1400 cm^{-1}. This is a common motif [8–13,61–79] in VTST calculations of atom-transfer reactions. The stretching vibration associated with the breaking bond correlates with the stretching vibration for the newly forming bond but shows a deep minimum at a geometry where both bonds have a bond order of about half. The resulting higher barrier on the V_a^G curve causes the lower rate for R2. We also can understand this issue from another point of view. The large decrease of the vibrational frequency of R1 at transition state compensates the higher potential energy barrier of R1, so that the number of accessible states of R1 is larger than that of R2 at the variational transition state and leads to the larger reaction rate for R1.

As would be expected, the branching ratios are quite sensitive to the barrier heights at low temperatures. For instance, M08-SO/ma-TZVP predicts branching ratio as 5.7 at 200 K, while M08–SO/6–311G(2*df*,2*p*) gives this ratio as 3.8 at 200 K. Figure 4 shows that branching ratios calculated with the two basis sets become very similar to each other above 1500 K; this is because the effective barrier difference becomes smaller compared to $k_B T$.

The tunneling contributions for both reactions are not as large as for many other hydrogen-transfer reactions because the barriers of two reactions are quite low and very broad. The SCT transmission coefficient κ is about 5–7 at 200 K for the two reactions, and it rapidly decreases to below 2 when the temperature is higher than 350 K. The V_a^G profiles of these two reactions are very similar in shape, and therefore the tunneling contributions are similar for the two reactions, even though the imaginary frequencies of the two reactions differ by a large factor (they are 1603*i* cm^{-1} for R1 and 916*i* cm^{-1} for R2). Consequently, even though the tunneling contribution is not large for these two reactions, the Wigner method (which was derived for small tunneling corrections, but which is essentially never recommended) incorrectly predicts the differential effect of tunneling on the two reactions. For the addition reaction, it gives a large error, in particular, it yields κ equal to 2.8 at $T = 200$ K, while the SCT approximation yields 6.2.

For reaction (R2), the Wigner method happens to give κ equal to 6.5 at 200 K. Although this agrees with the SCT value 6.2, this agreement is not a validation of the Wigner method; it is simply an accident since a Wigner tunneling factor of 6.5 corresponds to truncating a Taylor series after two terms when the first term is 1 and the second term should be small but is 5.5.

Note that transmission coefficient κ accounts for both multidimensional tunneling and nonclassical reflection. Usually, the tunneling effect dominates the nonclassical reflection effect because the former occurs at temperatures that have a large Boltzmann factor. However, this is not always the case, especially for reactions with low barriers. In the present case, the SCT transmission coefficient decreases the rate constant for both R1 and R2 at temperatures above 1400 K because nonclassical reflection has a larger effect than does tunneling at these temperatures.

To make it convenient to obtain the rate constant at arbitrary temperatures between 200 and 1500 K, we fit our calculated rate constants using the following formula,[80] which is an improvement over a formula presented previously:[81]

$$k = A \left(\frac{T + T_0}{300} \right)^n \exp \left[-\frac{E(T + T_0)}{R(T^2 + T_0^2)} \right], \qquad (4)$$

where k is rate constant, T is temperature, R is the gas constant, and A (in cm^3 molecule^{-1} s^{-1} for bimolecular reaction or in s^{-1} for unimolecular reaction), T_0 (in K), n, and E (in kcal mol^{-1}) are fitting parameters. This formula[80] is an improvement over the earlier one[81] because it has a more correct low-temperature limit. The resulting expressions for R1 and R2 (fitted to M08-SO/6-311++G(2*df*,2*p*) rate constants) are given by Eqs. (5) and (6), respectively, in units of cm^3 molecule^{-1} s^{-1} for A, kcal/mol for E, and K for T_0:

$$k_1 = 9.144 \times 10^{-12} \left(\frac{T + 146.54}{300} \right)^{1.357}$$
$$\times \exp \left[-\frac{0.8046(T + 146.54)}{R(T^2 + 2.147 \times 10^4)} \right], \qquad (5)$$

$$k_2 = 8.095 \times 10^{-12} \left(\frac{T + 148.85}{300} \right)^{1.490}$$
$$\times \exp \left[-\frac{1.220(T + 148.85)}{R(T^2 + 2.216 \times 10^4)} \right]. \qquad (6)$$

The expressions for R1 and R2 that are fitted to M08-SO/ma-TZVP rate constants are given by

$$k_1 = 7.965 \times 10^{-12} \left(\frac{T + 132.03}{300} \right)^{1.408}$$
$$\times \exp \left[-\frac{0.7372(T + 132.03)}{R(T^2 + 1.743 \times 10^4)} \right], \qquad (7)$$

$$k_2 = 7.678 \times 10^{-12} \left(\frac{T + 144.53}{300} \right)^{1.500}$$
$$\times \exp \left[-\frac{1.394(T + 144.53)}{R(T^2 + 2.089 \times 10^4)} \right]. \qquad (8)$$

IV. CONCLUDING REMARKS

In this article we presented a set of high-level *ab initio* calculations of the barrier heights of the abstraction and addition reactions of H with *trans*-N_2H_2, and we also calculated the rate constants of the two reactions by multistructural variational transition state theory with multidimensional tunneling and nonclassical reflection and including torsional anharmonicity. The abstraction reaction shows a very large variational effect due to the significant increase of one of the vibrational frequencies in the vicinity of the SP. The different sets of vibrational frequencies at the two competitive transition states cause the reaction to favor the one with the higher potential-energy barrier. This example clearly shows that it is important—in order to draw reliable conclusions about branching ratios and reaction mechanisms—to find the variational dynamical bottleneck that limits the reactive flux; restricting considerations only to barrier height calculations or conventional transition state theory is insufficient. Furthermore, it is necessary to consider the entire vibrationally adiabatic potential curve to predict the extent of tunneling; restricting consideration to the imaginary frequency at the saddle point is insufficient. The interesting features of the branching ratio predicted by theory prompt us to urge an experimental study of these reactions to confirm the predictions.

[1] D. G. Truhlar and B. C. Garrett, Acc. Chem. Res. **13**, 440 (1980).

[2] D. G. Truhlar and B. C. Garrett, Annu. Rev. Phys. Chem. **35**, 159 (1984).

[3] D. G. Truhlar, B. C. Garrett, and S. J. Klippenstein, J. Phys. Chem. **100**, 12771 (1996).

[4] A. Fernandez-Ramos, J. A. Miller, S. J. Klippenstein, and D. G. Truhlar, Chem. Rev. **106**, 4518 (2006).

[5] H. Eyring, J. Chem. Phys. **3**, 107 (1935).

[6] H. Eyring, Chem. Rev. **17**, 65 (1935).

[7] P. R. Schreiner, H. P. Reisenauer, D. Ley, D. Gerbig, C.-H. Wu, and W. D. Allen, Science **332**, 1300 (2011).

[8] B. C. Garrett and D. G. Truhlar, J. Am. Chem. Soc. **101**, 4534 (1979).

[9] B. C. Garrett, D. G. Truhlar, R. S. Grev, and A. W. Magnuson, J. Phys. Chem. **84**, 1730 (1980); **87**, 4554 (1983) [Erratum].

[10] B. C. Garrett and D. G. Truhlar, J. Am. Chem. Soc. **102**, 2559 (1980).

[11] B. C. Garrett, D. G. Truhlar, and R. S. Grev, in *Potential Energy Surfaces and Dynamics Calculations*, edited by D. G. Truhlar (Plenum, New York, 1981), pp. 587.

[12] D. G. Truhlar, A. D. Isaacson, R. T. Skodje, and B. C. Garrett, J. Phys. Chem. **86**, 2252 (1982).

[13] B. C. Garrett, D. G. Truhlar, A. F. Wagner, and T. H. Dunning, J. Chem. Phys. **78**, 4400 (1983).

[14] S. Wu and R. A. Marcus, J. Chem. Phys. **56**, 3519 (1972).

[15] D. G. Truhlar and A. Kuppermann, J. Chem. Phys. **56**, 2232 (1972).

[16] J. W. Duff and D. G. Truhlar, Chem. Phys. Lett. **23**, 327 (1973).

[17] Y.-Y. Chuang, E. L. Coitiño, and D. G. Truhlar, J. Phys. Chem. A **104**, 446 (1999).

[18] K. Raghavachari, G. W. Trucks, J. A. Pople, and M. Head-Gordon, Chem. Phys. Lett. **157**, 479 (1989).

[19] B. J. Lynch and D. G. Truhlar, J. Phys. Chem. A **105**, 2936 (2001).

[20] Y. Zhao, B. J. Lynch, and D. G. Truhlar, Phys. Chem. Chem. Phys. **7**, 43 (2005).

[21] D. P. Linder, X. Duan, and M. Page, J. Chem. Phys. **104**, 6298 (1996).

[22] Y.-Y. Chuang and D. G. Truhlar, J. Phys. Chem. A **101**, 3808 (1997).

[23] Y.-Y. Chuang and D. G. Truhlar, J. Chem. Phys. **107**, 83 (1997).

[24] D.-Y. Hwang and A. M. Mebel, J. Phys. Chem. A **107**, 2865 (2003).

[25] W.-P. Hu, Y.-P. Lu, and D. G. Truhlar, J. Chem. Soc., Faraday Trans. **90**, 1715 (1994).

[26] T. Yu, J. Zheng, and D. G. Truhlar, Chem. Sci. **2**, 2199 (2011).

[27] J. Zheng, T. Yu, E. Papajak, I. M. Alecu, S. L. Mielke, and D. G. Truhlar, Phys. Chem. Chem. Phys. **13**, 10885 (2011).

[28] M. Biczysko, L. A. Poveda, and A. J. C. Varandas, Chem. Phys. Lett. **424**, 46 (2006).

[29] T. H. Dunning, Jr., J. Chem. Phys. **90**, 1007 (1989).

[30] Y. Zhao and D. G. Truhlar, J. Chem. Theory Comput. **4**, 1849 (2008).

[31] J. Zheng, X. Xu, and D. G. Truhlar, Theor. Chim Acta **128**, 295 (2011).

[32] T. B. Adler, G. Knizia, and H.-J. Werner, J. Chem. Phys. **127**, 221106 (2007).

[33] G. Knizia, T. B. Adler, and H.-J. Werner, J. Chem. Phys. **130**, 054104 (2009).

[34] H.-J. Werner and P. J. Knowles, J. Chem. Phys. **89**, 5803 (1988).

[35] P. J. Knowles and H.-J. Werner, Chem. Phys. Lett. **145**, 514 (1988).

[36] E. R. Davidson, in *The World of Quantum Chemistry*, edited by R. Daudel and B. Pullman (Reidel, Dordrecht, 1974).

[37] S. R. Langhoff and E. R. Davidson, Int. J. Quantum Chem. **8**, 61 (1974).

[38] H.-J. Werner and P. J. Knowles, Theor. Chim Acta **78**, 175 (1990).

[39] R. J. Gdanitz and R. Ahlrichs, Chem. Phys. Lett. **143**, 413 (1988).

[40] P. G. Szalay and R. J. Bartlett, Chem. Phys. Lett. **214**, 481 (1993).

[41] A. Halkier, T. Helgaker, P. Jørgensen, W. Klopper, H. Koch, J. Olsen, and A. K. Wilson, Chem. Phys. Lett. **286**, 243 (1998).

[42] D. E. Woon and T. H. Dunning, J. Chem. Phys. **103**, 4572 (1995).

[43] J. M. L. Martin and P. R. Taylor, Chem. Phys. Lett. **248**, 336 (1996).

[44] P. L. Fast and D. G. Truhlar, J. Chem. Phys. **109**, 3721 (1998).

[45] I. M. Alecu, J. Zheng, Y. Zhao, and D. G. Truhlar, J. Chem. Theory Comput. **6**, 2872 (2010).

[46] D. G. Truhlar and A. Kuppermann, J. Am. Chem. Soc. **93**, 1840 (1971).

[47] D.-h. Lu, T. N. Truong, V. S. Melissas, G. C. Lynch, Y.-P. Liu, B. C. Garrett, R. Steckler, A. D. Isaacson, S. N. Rai, G. C. Hancock, J. G. Lauderdale, T. Joseph, and D. G. Truhlar, Comput. Phys. Commun. **71**, 235 (1992).

[48] Y.-P. Liu, G. C. Lynch, T. N. Truong, D.-h. Lu, D. G. Truhlar, and B. C. Garrett, J. Am. Chem. Soc. **115**, 2408 (1993).

[49] M. J. Frisch, G. W. Trucks, H. B. Schlegel *et al.*, GAUSSIAN 09 revision A.02, Gaussian, Inc., Wallingford, CT, 2009; Y. Zhao, R. Peverati, K. Yang, and D. G. Truhlar, MN-GFM version 5.0 (University of Minnesota, Minneapolis, 2011).

[50] H.-J. Werner, P. J. Knowles, F. R. Manby, M. Schütz, *et al.*, MOLPRO version 2010.1, a package of *ab initio* programs 2010.

[51] J. Zheng, S. Zhang, B. J. Lynch, J. C. Corchado, Y.-Y. Chuang, P. L. Fast, W.-P. Hu, Y.-P. Liu, G. C. Lynch, K. A. Nguyen, C. F. Jackels, A. F. Ramos, B. A. Ellingson, V. S. Melissas, J. Villà, I. Rossi, E. L. Coitino, J. Pu, T. V. Albu, R. Steckler, B. C. Garrett, A. D. Isaacson, and D. G. Truhlar, POLYRATE, University of Minnesota, Minneapolis, 2010.

[52] J. Zheng, S. L. Mielke, K. L. Clarkson, and D. G. Truhlar, Computer Phys. Commun. **183**, 1803 (2012).

[53] B. A. Ellingson, D. P. Theis, O. Tishchenko, J. Zheng, and D. G. Truhlar, J. Phys. Chem. A **111**, 13554 (2007).

[54] O. Tishchenko, J. Zheng, and D. G. Truhlar, J. Chem. Theory Comput. **4**, 1208 (2008).

[55] Y. Zhao, O. Tishchenko, J. R. Gour, W. Li, J. J. Lutz, P. Piecuch, and D. G. Truhlar, J. Phys. Chem. A **113**, 5786 (2009).

[56] O. Tishchenko, S. Ilieva, and D. G. Truhlar, J. Chem. Phys. **133**, 021102 (2010).

[57] T. J. Lee and P. R. Taylor, Int. J. Quantum Chem. Symp. **23**, 199 (1989).

[58] J. C. Rienstra-Kiracofe, W. D. Allen, and H. F. Schaefer, J. Phys. Chem. A **104**, 9823 (2000).

[59] G. S. Hammond, J. Am. Chem. Soc. **77**, 334 (1955).

[60] See supplementary material at http://dx.doi.org/10.1063/1.4707734 for more information about barrier heights, reaction energies, geometries, vibrational frequencies, vibrationally adiabatic potential curves, and rate constants.

[61] B. C. Garrett and D. G. Truhlar, J. Phys. Chem. **83**, 1079 (1979); **84**, 682–686 (1980) [Erratum]; **87**, 4553–4554 (1983).

[62] B. C. Garrett and D. G. Truhlar, J. Chem. Phys. **72**, 3460 (1980).

[63] B. C. Garrett, D. G. Truhlar, and A. W. Magnuson, J. Chem. Phys. **74**, 1029 (1981).

[64] B. C. Garrett, D. G. Truhlar, R. S. Grev, G. C. Schatz, and R. B. Walker, J. Phys. Chem. **85**, 3806 (1981).

[65] B. C. Garrett, D. G. Truhlar, and A. W. Magnuson, J. Chem. Phys. **76**, 2321 (1982).

[66] D. G. Truhlar and A. D. Isaacson, J. Chem. Phys. **77**, 3516 (1982).

[67] D. K. Bondi, J. N. L. Connor, B. C. Garrett, and D. G. Truhlar, J. Chem. Phys. **78**, 5981 (1983).

[68] D. G. Truhlar, R. S. Grev, and B. C. Garrett, J. Phys. Chem. **87**, 3415 (1983).

[69] S. C. Tucker, D. G. Truhlar, B. C. Garrett, and A. D. Isaacson, J. Chem. Phys. **82**, 4102 (1985).

[70] B. C. Garrett and D. G. Truhlar, J. Phys. Chem. **89**, 2204 (1985).

[71] B. C. Garrett, N. Abusalbi, D. J. Kouri, and D. G. Truhlar, J. Chem. Phys. **83**, 2252 (1985).

[72] B. C. Garrett and D. G. Truhlar, Int. J. Quantum Chem. **29**, 1463 (1986).

[73] B. C. Garrett, D. G. Truhlar, A. J. C. Varandas, and N. C. Blais, Int. J. Chem. Kinet. **18**, 1065 (1986).

[74] B. C. Garrett, D. G. Truhlar, J. M. Bowman, and A. F. Wagner, J. Phys. Chem. **90**, 4305 (1986).

[75] B. C. Garrett and D. G. Truhlar, Int. J. Quantum Chem. **31**, 17 (1987).

[76] T. Joseph, D. G. Truhlar, and B. C. Garrett, J. Chem. Phys. **88**, 6982 (1988).

[77] B. C. Garrett and D. G. Truhlar, J. Phys. Chem. **95**, 10374 (1991).

[78] V. S. Melissas and D. G. Truhlar, J. Chem. Phys. **99**, 1013 (1993).

[79] V. S. Melissas and D. G. Truhlar, J. Phys. Chem. **98**, 875 (1994).

[80] J. Zheng and D. G. Truhlar, Faraday Discuss. (in press).

[81] J. Zheng and D. G. Truhlar, Phys. Chem. Chem. Phys. **12**, 7782 (2010).